Methane Conversion

DOI: 10.1002/anie.201102320

Efficient Sunlight-Driven Dehydrogenative Coupling of Methane to Ethane over a Zn^{+}-Modified Zeolite**

*Lu Li, Guo-Dong Li, Chang Yan, Xiao-Yue Mu, Xiao-Liang Pan, Xiao-Xin Zou, Kai-Xue Wang, and Jie-Sheng Chen**

Effective conversion of methane to a mixture of more valuable hydrocarbons and hydrogen under mild conditions is a great scientific and practical challenge.[1–7] Up to date, the thermal routes for activation of the strong C–H bond (104 kcal mol^{-1}) in methane require high temperatures and multistep processes, and therefore they are energy-consuming and inefficient.[8,9] Compared to methods powered by thermal energy,[10–14] techniques that use photonic energy have substantial advantages, such as the capacity to minimize coking at room temperature. A promising approach to methane conversion is the direct non-oxidative coupling of methane (NOCM) to form ethane and hydrogen powered by photons [Equation (1)].[15,16]

$$2\,CH_4 \xrightarrow{h\nu} C_2H_6 + H_2 \qquad (1)$$

The produced ethane can in turn be conveniently converted to liquid fuels or ethene through metathesis and dehydrogenation, respectively.[17] Furthermore, this NOCM reaction is the best way to produce clean H_2 energy from fossil fuels because methane has the highest H/C ratio among all hydrocarbons. However, the methane conversion using photocatalysts previously reported for the NOCM reaction is very low (less than 4% upon UV irradiation for 90 hours).[18] More importantly, the wavelength of the light used in the photocatalytic systems previously reported for NOCM needs to be shorter than 270 nm, which is beyond the region of the solar spectrum (wavelength $\lambda > 290$ nm) reaching the surface of the Earth. To achieve a substantial yield and to exploit solar energy effectively, the development of photocatalytic systems with a distinctly higher activity, higher selectivity, and lower photon energy threshold is desired.

Herein, we report a Zn^{+}-modified ZSM-5 zeolite catalyst which exhibits superior photocatalytic activity for selective C–H activation of an alkane molecule and methane conversion both upon high-pressure irradiation of a mercury lamp and sunlight irradiation at room temperature. An optimized catalyst converts 24% of methane upon irradiation for 8 hours by a high-pressure mercury lamp with a selectivity larger than 99% for ethane and hydrogen products. Mechanistic studies suggest a two-stage photoexcitation process, which lowers the energy threshold ($\lambda < 390$ nm) needed to power our photocatalytic system relative to that ($\lambda < 270$ nm) required by previously reported systems.

Interactions of zeolites with metal vapors are an effective approach for the preparation of metal-containing zeolites.[19,20] Using this approach, we have synthesized a zinc-modified ZSM-5 catalyst with a Brunauer–Emmett–Teller (BET) surface area of 362 m^{2}g^{-1} through a solid–vapor reaction between a dehydrated HZSM-5 zeolite (protonated ZSM-5 with a Si/Al ratio of the framework of 14.8) and metallic zinc vapor. During the reaction, the protons of the Brønsted acidic sites (OH groups bridging Al and Si atoms of the framework) in the zeolite are reduced by zinc atoms to form H_2 molecules (as detected by gas chromatography, GC), whereas the zinc atoms undergo two different oxidation reactions, as demonstrated by our experimental observations. One reaction involves a zinc atom that reduce two closely positioned protons to form a Zn^{2+} cation; the other reaction is based on a zinc atom that reduces one isolated proton to form a Zn^{2+} cation with an extra electron delocalized on the zeolite framework. Delocalization of electrons on a zeolite framework has been reported previously,[21,22] and the delocalized electrons do not give rise to electron paramagnetic resonance (EPR) signals. For clarity, the corresponding as-prepared product is designated as Zn^{2+}-ZSM-5^{-}. According to inductively coupled plasma (ICP) elemental analysis, the composition of Zn^{2+}-ZSM-5^{-} is $Zn_{0.69}AlSi_{14.8}O_{31.6}$. Because the molar ratio of Zn/Al in the Zn^{2+}-ZSM-5^{-} material is 0.69, about 55% of the incorporated Zn atoms reduce one proton per Zn atom and the rest (45%) of the Zn atoms reduce two protons per Zn atom (see the Supporting Information). To further demonstrate the formation of Zn^{2+}-ZSM-5^{-}, we have also prepared a fully Zn^{2+}-exchanged ZMS-5 material (designated as Zn^{2+}-ZSM-5) for comparison through ion exchange of $Zn(NO_3)_2$ with NaZSM-5 in aqueous solution followed by evacuation at 500 °C to remove the adsorbed water molecules. The composition of the reference Zn^{2+}-ZSM-5 is $Zn_{0.49}AlSi_{14.8}O_{31.6}$ according to the ICP analysis.

Both Zn^{2+}-ZSM-5^{-} and Zn^{2+}-ZSM-5 in vacuum are EPR-silent, indicating that no localized unpaired electrons are present in these two samples. However, after irradiation of ultraviolet (UV) light from a 150 W high-pressure Hg lamp

[*] L. Li, Prof. K. X. Wang, Prof. J. S. Chen
School of Chemistry and Chemical Engineering
Shanghai Jiao Tong University
Shanghai 200240 (People's Republic of China)
E-mail: chemcj@sjtu.edu.cn
L. Li, Prof. G. D. Li, C. Yan, X. Y. Mu, X. L. Pan, X. X. Zou
State Key Laboratory of Inorganic Synthesis
and Preparative Chemistry
College of Chemistry, Jilin University
Changchun 130012 (People's Republic of China)

[**] This work was financially supported by the NSFC of China, the National Basic Research Program of China, and the Graduate Innovation Fund of Jilin University.

Supporting information for this article is available on the WWW under http://dx.doi.org/10.1002/anie.201102320.

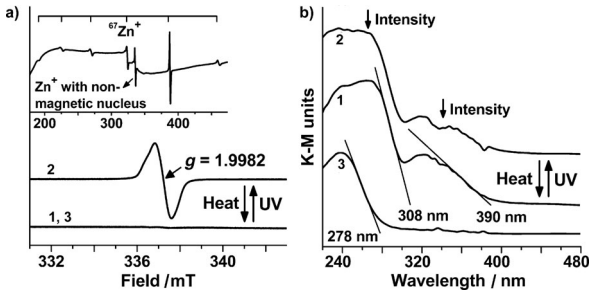

Figure 1. a) Room-temperature X-band EPR spectra and b) UV/Vis diffuse reflectance spectra of the Zn^{2+}-ZSM-5$^-$ sample in vacuum (curve 1), the (Zn^+,Zn^{2+})-ZSM-5$^-$ sample (curve 2), and the reference Zn^{2+}-ZSM-5 sample (curve 3; K-M units = Kubelka-Munk units). The inset of Figure 1 a is the EPR spectrum of the ^{67}(Zn^+,Zn^{2+})-ZSM-5$^-$ sample. The EPR spectrum for the reference Zn^{2+}-ZSM-5 material (curve 3) is identical to that for Zn^{2+}-ZSM-5$^-$ (curve 1).

for one hour, the initially EPR-silent Zn^{2+}-ZSM-5$^-$ probe shows an intense EPR signal characteristic of the Zn^+ cation (Figure 1 a), which is stable and undergoes no variations in vacuum for at least 18 months at room temperature. The presence of Zn^+ cations in the UV-irradiated material is confirmed by using a ^{67}Zn(I=5/2)-enriched source (97 %) to react with HZSM-5. After irradiation, the EPR spectrum of the $^{67}Zn^{2+}$-ZSM-5$^-$ sample exhibits six hyperfine lines because of the interaction of the unpaired 4s electron of $^{67}Zn^+$ with the $I = 5/2$ nuclear spin (see Figure S1 in the Supporting Information). The slightly negative g shift and the large hyperfine splitting also agree with previously reported data for the EPR spectrum of the Zn^+ ion.[23] The concentration of the Zn^+ cations in the sample is 0.062 mmol g^{-1} according to electron spin concentration measurements (see Figure S2 in the Supporting Information). We attribute the formation of the Zn^+ species to a photo-induced one-electron transfer from the zeolite framework to the 4s orbital of the Zn^{2+} cation in the as-prepared Zn^{2+}-ZSM-5$^-$ sample. The corresponding UV-irradiated sample is designated as (Zn^+,Zn^{2+})-ZSM-5$^-$ accordingly. The 4s electron of the Zn^+ cation falls back to the zeolite framework under thermal treatment in the absence of UV irradiation. At above 220 °C, the photoinduced EPR signal of the Zn^+ cation disappears completely (Figure 1 a), but this signal reappears after the sample has been irradiated a second time. As expected, no EPR signal is observed for the reference Zn^{2+}-ZSM-5 sample after UV-irradiation because there are no extra delocalized electrons on the zeolite framework in this case.

To pinpoint the nature of the zinc-containing material, a series of further experiments were conducted. The UV/Vis diffuse reflectance spectra of both Zn^{2+}-ZSM-5$^-$ and (Zn^+,Zn^{2+})-ZSM-5$^-$ show three absorption thresholds at 390, 308, and 278 nm (Figure 1 b and Figure S3 in the Supporting Information). The intensity of the absorption bands between 390 and 278 nm for (Zn^+,Zn^{2+})-ZSM-5$^-$ is slightly diminished relative to those bands for Zn^{2+}-ZSM-5$^-$, whereas the absorption band below 278 nm assigned to framework Al–O units[24] is not affected by UV irradiation. For comparison, the reference Zn^{2+}-ZSM-5 sample shows only one absorption band of framework Al–O units. These spectroscopic observations further support the presence of extra electrons on the framework of the as-prepared Zn^{2+}-ZSM-5$^-$ material. The transition of these extra electrons to the 4s orbitals of the Zn^{2+} cations is responsible for the optical absorption in the range of 390 and 278 nm. In fact, the electron undergoes a dynamic equilibrium between the zeolite framework and the 4s orbitals of Zn^{2+} cations upon UV irradiation, and as a result only a very limited number of the extra delocalized electrons are excited from the zeolite framework to the Zn^{2+} 4s orbitals by UV light. This is in agreement with the fact that the intensity of the absorption band of (Zn^+,Zn^{2+})-ZSM-5$^-$ between 390 and 278 nm does not change much in comparison with that of the as-prepared Zn^{2+}-ZSM-5$^-$.

The photocatalytic performance of the (Zn^+,Zn^{2+})-ZSM-5$^-$ sample for methane conversion was tested at room temperature upon irradiation from either a 150 W high-pressure Hg lamp and sunlight. The catalyst was spread evenly on the wall of an airtight quartz reactor in vacuum (see Figure S4 in the Supporting Information), followed by introduction of a specific quantity (1000 and 200 μmol) of pure methane (> 99.995 %). We found that the (Zn^+,Zn^{2+})-ZSM-5$^-$ catalyst formed through photoirradiation of Zn^{2+}-ZSM-5$^-$ was rather active for selective C–H bond activation of methane and for the NOCM reaction upon irradiation with both light sources. The catalytic reaction led to the formation of ethane with nearly equimolar amounts of H_2 (see Table S1 in the Supporting Information). Carbon mass balances during the conversion were close to 100 % and no carbon oxides were detected by gas chromatography. Figure 2 a shows the time courses of H_2 evolution from methane over 1.0 g of (Zn^+,Zn^{2+})-ZSM-5$^-$ upon irradiation with both light sources. To avoid the influence of varying methane concentrations, the amount of methane chosen for this reaction was large (1000 μmol). According to the data, the activity of (Zn^+,Zn^{2+})-ZSM-5$^-$ showed no noticeable degradation after 16 h of irradiation. The total amount of H_2 released upon UV

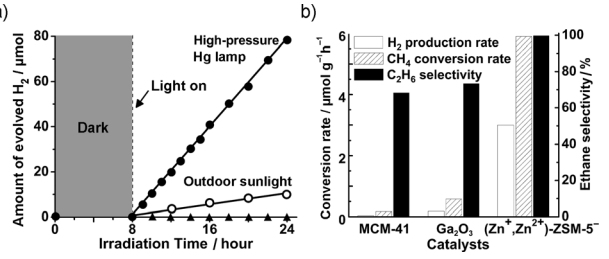

Figure 2. a) Photocatalytic hydrogen evolution as a function of time obtained at room temperature in the non-oxidative coupling of methane (NOCM) reaction catalyzed by (Zn^+,Zn^{2+})-ZSM-5$^-$ upon high-pressure irradiation of the Hg lamp at an intensity of 100 mW cm^{-2} (full circles) and sunlight irradiation at an intensity of around 50 mW cm^{-2} (empty circles). The activity of the reference Zn^{2+}-ZSM-5 sample upon high-pressure irradiation of the Hg lamp is negligible (full triangles). b) Methane conversion rate, hydrogen production rate, and ethane selectivity obtained for the NOCM reaction catalyzed by different photocatalysts upon direct irradiation from a high-pressure Hg lamp over 8 h. An amount of 1000 μmol of methane was used in (a) and 200 μmol in (b); 1.0 g of catalyst was used in all cases.

irradiation from the high-pressure Hg lamp for 16 h was measured by gas chromatography to be 78.3 μmol, which corresonds to an H_2 production rate of 4.9 $\mu mol\,h^{-1}\,g^{-1}$ and an associated methane conversion rate of around 9.8 $mmol\,h^{-1}\,g^{-1}$. On the basis of the Zn^+ concentration (0.062 μmol g), the turnover number (TON) for the (Zn^+,Zn^{2+})-ZSM-5$^-$ material was about 2526 for a reaction time of 16 h, corresponding to a turnover frequency (TOF) of 158 h^{-1}. In contrast, the ternary SiO_2-Al_2O_3-TiO_2 material, which is the most effective photocatalyst previously reported for NOCM, exhibits a methane conversion rate of 1.3 $\mu mol\,h^{-1}\,g^{-1}$ under similar conditions.[15] More importantly, if sunlight ($\lambda > 290$ nm) is used as light source, (Zn^+,Zn^{2+})-ZSM-5$^-$ still exhibits considerable efficiency for the NOCM reaction (Figure 2a), whereas none of the previously reported materials shows photocatalytic activity under these conditions.[16]

The reusability of (Zn^+,Zn^{2+})-ZSM-5$^-$ was tested for four catalytic cycles (see Figure S5 in the Supporting Information). After the test, the crystal structure of the catalyst sample remained intact as judged by powder X-ray diffraction (see Figure S6 in the Supporting Information), and no carbon-containing deposits were retained in the zeolite as demonstrated by IR, in situ EPR spectroscopies (see Figure S7 in the Supporting Information), and elemental analysis. The testing result indicated that the catalyst could be used repeatedly without noticeable deactivation in the absence of moisture. In the presence of moisture, the photocatalytic activity of (Zn^+,Zn^{2+})-ZSM-5$^-$ for NOCM decreased to a certain extent, depending on the content of water in the reaction system (see Figure S8 in the Supporting Information).

The selectivity for ethane over alternative hydrocarbon products (propane, butane, etc.) was measured by gas chromatography to be 99.6% upon irradiation by the high-pressure Hg lamp and >99.9% upon sunlight irradiation. When photocatalytic coupling was attempted using pure ethane instead of methane as the reactant, neither butane nor hydrogen was observed (see Figure S9 in the Supporting Information). This result indicates that the formation of butane from ethane coupling is unfavorable at room temperature because the medium pores (diameter of 0.55 nm) of ZSM-5 are not large enough for two ethane molecules to interact with each other at the Zn^+ active site in the zeolite pore. In contrast, Zn^+-modified zeolites (such as zeolite Y) with a larger pore diameter (cage diameter of 1.0 nm and window diameter of 0.74 nm) activate ethane (see Figure S10 in the Supporting Information), suggesting that the shape selectivity of the zeolite framework structure plays a crucial role in room-temperature photocatalytic conversion of hydrocarbons. In addition, the reaction does not proceed in the dark and in the absence of Zn^+ cations (exemplified by the reference Zn^{2+}-ZSM-5 material), confirming that the coupling of methane to ethane by (Zn^+,Zn^{2+})-ZSM-5$^-$ is a photocatalytic process and the Zn^+ cations are the photocatalytic active sites.

To assess the performance of (Zn^+,Zn^{2+})-ZSM-5$^-$ further, Ga_2O_3[25] and the mesoporous silica MCM-41[26] (see Figure S11 in the Supporting Information), two effective photocatalysts reported previously for the NOCM reaction upon irradiation at shorter UV wavelength ($\lambda < 270$ nm), were prepared and tested for comparison (these two materials are more easily available than the ternary SiO_2-Al_2O_3-TiO_2 material). Using 1.0 g of the catalyst and 200 mmol of methane (standard conditions described in Figure 2b and in Table S2 in the Supporting Information), we obtained conversion rates for methane of 0.58 $\mu mol\,h^{-1}\,g^{-1}$ over Ga_2O_3 and 0.17 $\mu mol\,h^{-1}\,g^{-1}$ over MCM-41 upon UV irradiation from the high-pressure Hg lamp, respectively. In contrast, a conversion rate of methane of 6.0 $\mu mol\,h^{-1}\,g^{-1}$ was achieved using the (Zn^+,Zn^{2+})-ZSM-5$^-$ catalyst under identical conditions (Figure 2b). To quantitatively evaluate the photocatalytic activities of Ga_2O_3 (and MCM-41) and (Zn^+,Zn^{2+})-ZSM-5$^-$ upon UV irradiation within the wavelength range of 300–400 nm, a UV-D35 filter (see Figure S12 in the Supporting Information) was carefully mounted in the system to completely block wavelengths shorter than 300 nm and longer than 400 nm from the high-pressure Hg lamp. Using 1.0 g of (Zn^+,Zn^{2+})-ZSM-5$^-$ and 200 μmol of methane, a conversion of 17.5% and an ethane selectivity of nearly 100% were achieved after irradiation for 24 h (see Figures S13 and S14 in the Supporting Information), and the quantum efficiency was calculated to be around 0.55%. In contrast, Ga_2O_3 (or MCM-41) did not show a photocatalytic activity at all under identical reaction conditions.

Upon irradiation with visible light ($\lambda > 400$ nm), the photocatalytic activity of (Zn^+,Zn^{2+})-ZSM-5$^-$ for NOCM was gradually reduced, and no activity was observed after 8 h of irradiation of visible light. Further inspection revealed that under visible light irradiation in the presence of methane, the (Zn^+,Zn^{2+})-ZSM-5$^-$ material became EPR-silent within 8 h, whereas in the absence of methane, the EPR signal persisted, indicating that there is a chance for the electron of the Zn^+ cation to fall back to the zeolite framework during the interaction with methane. However, upon re-excitation by UV irradiation from a 150 W high-pressure Hg lamp for 2 h, the EPR-silent sample regains its photocatalytic activity. As discussed earlier, the single electron transfer from the zeolite framework to the 4s orbital of the Zn^{2+} cation corresponds to UV absorption between 390 nm and 278 nm, and the energy of the irradiated visible light is not sufficient to drive this electron transfer. Therefore, UV irradiation ($\lambda < 390$ nm) must be used to proceed the photocatalytic reaction continuously. These observations suggest a two-stage catalytic process that requires light of wavelengths shorter than 390 nm to transfer electrons from the zeolite framework to the Zn^{2+} centers, and light of visible wavelengths to promote the Zn^+ reactivity towards methane. Using visible light of different wavelengths, we have found that the minimum energy required to drive the electron from the Zn^+ center to activate methane corresponds to a wavelength of about 700 nm. A schematic energy diagram for the whole processes involved in the photocatalytic reaction is given in Figure 3a.

Quantum chemical calculations give rise to the optimized structure of the initially adsorbed methane molecule linked to a Zn^+ cation in the pore of zeolite ZSM-5 (Figure 3b). According to the calculations, three hydrogen atoms of the methane molecule are attracted by the Zn^+ cation and the fourth hydrogen is on the opposite side. Presumably, upon

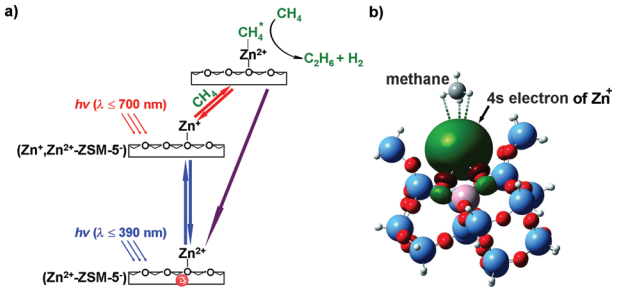

Figure 3. a) Schematic energy diagram for the processes of the photocatalytic reaction. b) The B3LYP hybrid exchange-correlation optimized geometry of the adsorbed methane molecule attracted by the Zn^+ active site (red: O, blue: Si, pink: Al, gray: C, white: H, and green: the 4s electron of Zn^+).

light irradiation ($\lambda < 700$ nm), the 4s electron of the Zn^+ cation is photoexcited to an empty C–H σ*-antibonding orbital of methane to active the C–H bond, followed by the attack of a second CH_4 molecule to accomplish the dehydrogenation coupling reaction. This process must be very fast because we did not observe a variation of the complex formed of methane and (Zn^+,Zn^{2+})-ZSM-5$^-$ during the photocatalytic reaction by in situ EPR and Raman spectroscopies (see Figure S15 in the Supporting Information).

The photocatalytic performance of the (Zn^+,Zn^{2+})-ZSM-5$^-$ catalyst depends on the Si/Al ratio (14.8 to ∞) of the zeolite framework (see Table S2 entries 1 to 4 in the Supporting Information). We found that the lower the content of Zn^+ cations is (higher Si/Al ratio), the lower is the conversion of methane. The highest methane conversion reached 23.8% for a catalyst sample with a Si/Al ratio of 14.8 (ZSM-5 with a lower Si/Al ratio is not available) under the standard conditions described in Table S2 (Figure S16 and S17) in the Supporting Information. As the Si/Al ratio for the (Zn^+,Zn^{2+})-ZSM-5$^-$ material is increased, not only the methane conversion but also the TOF value diminishes. The TOF decrease implies that when the Si/Al ratio increases in the zeolite, the relative number of accessible Zn^+ sites for NOCM gradually decreases. Zeolite Hβ and zeolite HY have also been used as host materials for the preparation of Zn^+-containing photocatalysts (see Figures S10 and S18 in the Supporting Information). The photocatalytic activities of the corresponding (Zn^+,Zn^{2+})-β$^-$ and (Zn^+Zn^{2+})-Y$^-$ samples are lower than that of (Zn^+,Zn^{2+})-ZSM-5$^-$ (see Table S2, entries 5 and 6 in the Supporting Information), suggesting that the framework structure of the zeolite host, which may influence the diffusion rate of the reactants and products, binding energy, and transition state of the complex formed by methane and Zn^+ during the photocatalytic process, also affect the photocatalytic conversion of methane.

The key to the performance of the (Zn^+,Zn^{2+})-ZSM-5$^-$ photocatalyst is the presence of univalent zinc species in the material. Unlike conventional photocatalysts for methane conversion, the catalytic activities of which rely on transient photoexcited electrons and holes, the Zn^+-modified zeolite photocatalyst takes advantage of the longer lifetime of the valence electrons of the Zn^+ species to activate the C–H bond of methane, and as a result, the solar spectrum reaching the Earth's surface may be exploited to power the NOCM reaction.

Experimental Section

Preparation of Zn^{2+}-ZSM-5$^-$, Zn^{2+}-β$^-$, and Zn^{2+}-Y$^-$: The details for the preparation of the zinc-containing photocatalysts are described in the Supporting Information.

Photocatalytic test: The (Zn^+,Zn^{2+})-ZSM-5$^-$ catalyst was air- and moisture-sensitive. To prevent the catalyst from deactivation by air and moisture, all the photocatalytic tests were performed under dry Ar atmosphere and vacuum using Schlenk glassware, glovebox, and vacuum-line techniques. All the reactants were dried by passing the corresponding gases through a column of $MgSO_4$ and $CuSO_4$ prior to catalytic testing. After reactions, the resulting zeolite samples were taken out from the reactor in the glove box, and for the following characterization the samples were always kept under argon. The photocatalytic activity for the non-oxidative coupling of methane to ethane was evaluated in an airtight quartz reactor (25 cm^3) at room temperature. The catalyst sample (1.0 g) was spread evenly on the wall of the closed quartz reactor in vacuum, followed by reaction with pure methane (200 and 1000 mmol) upon UV irradiation from a 150 W high-pressure Hg lamp (and sunlight) for 8 to around 24 h. The light intensities of the high-pressure Hg lamp and sunlight were around 100 and 50 mW cm^{-2}, respectively. If the UV-D35 filter ($300\text{ nm} < \lambda_{trans} < 400$ nm; trans: transmittance) was used, the light intensities measured at wavelengths between 300 and 400 nm were around 2.5 mW cm^{-2} for the high-pressure Hg lamp and around 2.0 mW cm^{-2} for sunlight. The hydrocarbon products were thermally desorbed by heating the catalyst gradually to 300 °C, which was kept for 60 min under evacuation, collected with a liquid-N_2 trap, and analyzed by gas chromatography (GC) with a flame ionization detector (FID). The amount of produced hydrogen was directly measured by GC with a thermal conductivity detector (TCD).

General characterization: The powder X-ray diffraction (XRD) patterns were recorded on a Rigaku D/Max 2550 X-ray diffractometer with Cu Kα radiation ($\lambda = 1.5418$ Å). The electron paramagnetic resonance spectra were obtained on a JES-FA 200 EPR spectrometer. The details of the instrumental parameters are as follows: scanning frequency: 9.45 GHz, central field: 3360 G, scanning width: 8000 G, scanning power: 0.998 mW, and scanning temperature: 25 °C. The stable radical 2,2-diphenyl-1-picrylhydrazyl (DPPH) and manganese (Mn) marker were used as standards for calculation of the spin concentration. For in situ UV/Vis diffuse reflectance spectroscopy measurements, the powder sample was sandwiched evenly between two quartz plates of a home-made airtight quartz cell under argon. When the sample was evacuated and exposed to methane, it was lowered from the preheating zone into the sample compartment for optical measurement. All the UV/Vis diffuse reflectance spectra were recorded on a Perkin–Elmer Lambda 20 UV/Vis spectrometer, whereas the UV/Vis absorption spectrum of the filter was measured with a Shimadzu UV-2450 spectrophotometer. The absorbance spectra were obtained from the reflectance spectra through Kubelka-Munk transformation. The FTIR spectra were recorded on a Bruker IFS 66v/S FTIR spectrometer equipped with a deuterated triglycine sulfate (DTGS) detector. The Raman spectra were obtained with a Renishaw inVia confocal Raman spectrometer and radiation at 532 nm from a solid-state laser was used as exciting source. The power of the laser was 350 mW. The ICP elemental analyses were performed on a Perkin–Elmer Optima 3300DV ICP spectrometer. The ^{29}Si magic angle spinning (MAS) NMR measurements were performed on a Varian Infinity plus 400 NMR spectrometer, and the Brunauer–Emmett–Teller (BET) surface areas of the

samples were measured from the adsorption of N_2 at 77 K by using a Micromeritics ASAP 2020 M system.

Received: April 4, 2011
Revised: June 28, 2011
Published online: July 14, 2011

Keywords: C–H activation · electron transfer · photocatalysis · zeolites · zinc

[1] J. H. Lunsford, *Catal. Today* **2000**, *63*, 165 – 174.
[2] R. A. Periana, O. Mironov, D. Taube, G. Bhalla, C. J. Jones, *Science* **2003**, *301*, 814 – 818.
[3] A. Holmen, *Catal. Today* **2009**, *142*, 2 – 8.
[4] J. M. Basset, C. Copéret, D. Soulivong, M. Taoufik, J. T. Cazat, *Acc. Chem. Res.* **2010**, *43*, 323 – 334.
[5] J. Lelieveld, S. Lechtenböhmer, S. S. Assonov, C. A. M. Brenninkmeijer, C. Dienst, M. Fischedick, T. Hanke, *Nature* **2005**, *434*, 841 – 842.
[6] R. G. Bergman, *Nature* **2007**, *446*, 391 – 393.
[7] R. Balasubramanian, S. M. Smith, S. Rawat, L. A. Yatsunyk, T. L. Stemmler, A. C. Rosenzweig, *Nature* **2010**, *465*, 115 – 119.
[8] H. D. Gesser, N. R. Hunter, C. B. Prakash, *Chem. Rev.* **1985**, *85*, 235 – 244.
[9] H. Arakawa, M. Aresta, J. N. Armor, M. A. Barteau, E. J. Beckman, A. T. Bell, J. E. Bercaw, C. Creutz, E. Dinjus, D. A. Dixon, K. Domen, D. L. Dubois, J. Eckert, E. Fujita, D. H. Gibson, W. A. Goddard, D. W. Goodman, J. Keller, G. J. Kubas, H. H. Kung, J. E. Lyons, L. E. Manzer, T. J. Marks, K. Morokuma, K. M. Nicholas, R. Periana, L. Que, J. Rostrup-Nielson, W. M. H. Sachtler, L. D. Schmidt, A. Sen, G. A. Somorjai, P. C. Stair, B. R. Stults and W. Tumas, *Chem. Rev.* **2001**, *101*, 953 – 996.
[10] V. R. Choudhary, A. K. Kinage, T. V. Choudhary, *Science* **1997**, *275*, 1286 – 1288.
[11] H. Zheng, D. Ma, X. H. Bao, J. Z. Hu, J. H. Kwak, Y. Wang, Charles H. F. Peden, *J. Am. Chem. Soc.* **2008**, *130*, 3722 – 3723.
[12] M. V. Luzgin, V. A. Rogov, S. S. Arzumanov, A. V. Toktarev, A. G. Stepanov, V. N. Parmon, *Angew. Chem.* **2008**, *120*, 4635 – 4638; *Angew. Chem. Int. Ed.* **2008**, *47*, 4559 – 4562.
[13] D. Soulivong, S. Norsic, M. Taoufik, C. Copéret, J. T. Cazat, S. Chakka, J. M. Basset, *J. Am. Chem. Soc.* **2008**, *130*, 5044 – 5045.
[14] K. C. Szeto, S. Norsic, L. Hardou, E. Le Roux, S. Chakka, J. Thivolle-Cazat, A. Baudouin, C. Papaioannou, J. M. Basset, M. Taoufik, *Chem. Commun.* **2010**, *46*, 3985 – 3987.
[15] L. Yuliati, H. Yoshida, *Chem. Soc. Rev.* **2008**, *37*, 1592 – 1602.
[16] K. Shimura, S. Kato, T. Yoshida, H. Itoh, T. Hattori, H. Yoshida, *J. Phys. Chem. C* **2010**, *114*, 3493 – 3503.
[17] S. F. Håkonsen, A. Holmen in *Handbook of Heterogeneous Catalysis,* (Eds.: G. Ertl, H. Knözinger, F. Schüth, J. Weitkamp), *Vol. 7*, Wiley-VCH, Weinheim, **2008**, pp. 3384 – 3400.
[18] H. Yoshida, N. Matsushita, Y. Kato, T. Hattori, *J. Phys. Chem. B* **2003**, *107*, 8355 – 8362.
[19] Y. S. Park, Y. S. Lee, K. B. Yoon, *J. Am. Chem. Soc.* **1993**, *115*, 12220 – 12221.
[20] A. Hagen, E. Schneider, A. Kleinert, F. Roessner, *J. Catal.* **2004**, *222*, 227 – 237.
[21] H. Garcia, H. D. Roth, *Chem. Rev.* **2002**, *102*, 3947 – 4007.
[22] L. Li, X. S. Zhou, G. D. Li, X. L. Pan, J. S. Chen, *Angew. Chem.* **2009**, *121*, 6806 – 6810; *Angew. Chem. Int. Ed.* **2009**, *48*, 6678 – 6682.
[23] F. F. Popescu, V. V. Crecu, *Solid State Commun.* **1973**, *13*, 749 – 751.
[24] E. D. Garbowski, C. Mirodatos, *J. Phys. Chem.* **1982**, *86*, 97 – 102.
[25] L. Yuliati, T. Hattori, H. Itoh, H. Yoshida, *J. Catal.* **2008**, *257*, 396 – 402.
[26] L. Yuliati, M. Tsubota, A. Satsuma, H. Itoh, H. Yoshida, *J. Catal.* **2006**, *238*, 214 – 220.

